JACS
JOURNAL OF THE AMERICAN CHEMICAL SOCIETY



Article

# Interfacial Charge Recombination Between e#TiO and the I/I Electrolyte in Ruthenium Heteroleptic Complexes: Dye Molecular Structure#Open Circuit Voltage Relationship

Anna Reynal, Amparo Forneli, Eugenia Martinez-Ferrero, Antonio Sa#nchez-Di#az, Anto#n Vidal-Ferran, Brian C. O'Regan, and Emilio Palomares

*J. Am. Chem. Soc.*, **2008**, 130 (41), 13558-13567 • DOI: 10.1021/ja800513m • Publication Date (Web): 20 September 2008



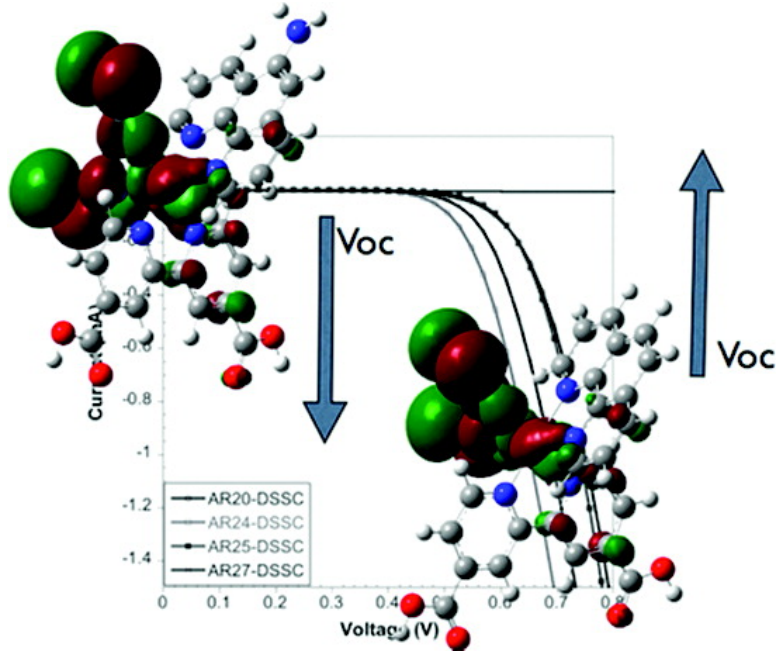


## More About This Article

Additional resources and features associated with this article are available within the HTML version:

- Supporting Information
- Access to high resolution figures
- Links to articles and content related to this article
- Copyright permission to reproduce figures and/or text from this article



Journal of the American Chemical Society is published by the American Chemical Society. 1155 Sixteenth Street N.W., Washington, DC 20036

J|A|C|S
ARTICLES

Published on Web 09/20/2008

# Interfacial Charge Recombination Between $e^-$−$TiO_2$ and the $I^-/I_3^-$ Electrolyte in Ruthenium Heteroleptic Complexes: Dye Molecular Structure−Open Circuit Voltage Relationship

Anna Reynal,[‡] Amparo Forneli,[‡] Eugenia Martinez-Ferrero,[‡] Antonio Sánchez-Díaz,[‡] Antón Vidal-Ferran,[†,‡] Brian C. O'Regan,[§] and Emilio Palomares*[,†,‡]

*ICREA and Institute of Chemical Research of Catalonia (ICIQ), Avda. Països Catalans 16, Tarragona, Spain, and Chemistry Department, Imperial College of London, South Kensington, Exhibition Road, SW7 2AZ London, United Kingdom*

Received January 22, 2008; E-mail: epalomares@iciq.es

***Abstract:*** A series of heteroleptic ruthenium(II) polypyridyl complexes containing phenanthroline ligands have been designed, synthesized, and characterized. The spectroscopic and electrochemical properties of the complexes have been studied in solution and adsorbed onto semiconductor nanocrystalline metal oxide particles. The results show that for two of the ruthenium complexes, bearing electron-donating (−$NH_2$) or electron-withdrawing (−$NO_2$) groups, the presence of the redox-active $I^-/I_3^-$ electrolyte produces important changes in the interfacial charge transfer processes that limit the device performance. For example, those dyes enhanced the electron recombination reaction between the photoinjected electrons at $TiO_2$ and the oxidized redox electrolyte. In an effort to understand the details of such striking observations, we have monitored the charge transfer reactions taking place at the different interfaces of the devices using time-resolved single photon counting, laser transient spectroscopy, and light-induced photovoltage measurements.

## Introduction

Ruthenium(II) polypyridyl complexes have been widely investigated as efficient light harvesting molecules in dye-sensitized solar cells (DSSCs).[1−3] In fact, devices made using as the sensitizer the complex *cis*-bis(isothiocyanato)bis(2,2′-bipyridyl-4,4′-dicarboxylato)ruthenium(II) bis(tetrabutylammonium), also known as N719 (Scheme 1), have achieved certified efficiencies for light-to-energy conversion of 11% under illumination at 1 sun (100 mW/cm$^2$).[4] Several groups have designed and synthesized a wide range of ruthenium(II) complexes, but still bis(2,2′-bipyridyl-4,4′-dicarboxylato)-based ruthenium complexes or their derivates have superior performance when compared in similar conditions, although a few exceptions have been demonstrated in recent years.[5−7] However, although it has been possible to achieve a higher photocurrent for devices made using those alternative dyes (for example, the "black dye",[7] chemical name tris(isothiocyanato)ruthenium(II) 2,2′:6′,2″-terpyridine-4,4′,4″- tricarboxylic acid, tris(tetrabutylammonium) salt), usually a decrease in the cell open circuit voltage ($V_{oc}$) has been observed.

A detailed study of the charge transfer reactions taking place at the different interfaces of a DSSC sensitized with N719 shows that electron transfer reactions are very much optimized.[8−12] For example, in a typical DSSC using an iodine/iodide liquid electrolyte, upon light absorption (Scheme 1, reaction 1) electron injection occurs in <1 ps to hundreds of picoseconds (Scheme 1, reaction 2). This is usually much faster than the nanosecond scale lifetime of excited ruthenium complexes in pure solution (Scheme 1, reaction 3). This normally gives an electron injection yield higher than 90%. Similarly, the oxidized dye is regenerated by the iodine/iodide electrolyte in 0.1−10 $\mu$s (Scheme 1, reaction 6), well before the back electron transfer reaction between the photoinjected electrons and the oxidized dye, which takes place in the range of hundreds of microseconds or even a few milliseconds (Scheme 1, reaction 4).

† ICREA.
‡ ICIQ.
§ Imperial College of London.

(1) Gratzel, M. *Prog. Photovoltaics* **2000**, *8*, 171–185.
(2) Kong, F.-T.; Dai, S.-Y.; Wang, K.-J. *Adv. Optoelectron.* **2007**, 1–13.
(3) Robertson, N. *Angew. Chem., Int. Ed.* **2006**, *45*, 2338.
(4) Chiba, Y.; Islam, A.; Watanabe, R.; Komiya, R.; Koide, N.; Han, L. *Jpn. J. Appl. Phys., Part 2* **2006**, *45*, L638.
(5) Kuang, D.; Klein, C.; Ito, S.; Moser, J.-E.; Humphry-Baker, R.; Zakeeruddin, S. M.; Gratzel, M. *Adv. Funct. Mater.* **2007**, *17*, 154.
(6) Nazeeruddin, M. K.; Pechy, P.; Renouard, T.; Zakeeruddin, S. M.; Humphry-Baker, R.; Comte, P.; Liska, P.; Cevey, L.; Costa, E.; Shklover, V.; Spiccia, L.; Deacon, G. B.; Bignozzi, C. A.; Gratzel, M. *J. Am. Chem. Soc.* **2001**, *123*, 1613–1624.
(7) Wang, Z. -S.; Yamaguchi, T.; Sugihara, H.; Arakawa, H. *Langmuir,* **2005**, *21*, 4272–4276.
(8) Anderson, N.; Lian, T. *Coord. Chem. Rev.* **2004**, *248*, 1231.
(9) Durrant, J. R.; Haque, S.; Palomares, E. *Coord. Chem. Rev.* **2004**, *248*, 1247.
(10) Ghosh, H. N.; Asbury, J. B.; Wneg, Y.; Lian, T. *J. Phys. Chem. B* **1998**, *102*, 10208.
(11) Haque, S.; Palomares, E.; Cho, B.; Green, A.; Hirata, N.; Klug, D.; Durrant, J. R. *J. Am. Chem. Soc.* **2005**, *127*, 3456.
(12) Weng, Y.-X.; Wang, Y.-Q.; Asbury, J. B.; Ghosh, H. N.; Lian, T. *J. Phys. Chem. B* **2000**, *104*, 93.
(13) Barolo, C.; Nazeeruddin, M. K.; Fantacci, S.; Di Censo, D.; Comte, P.; Liska, P.; Viscardi, G.; Quagliotto, P.; De Angelis, F.; Grätzel, M. *Inorg. Chem.* **2006**, *45*, 4642.
(14) Zhang, Z. P.; Evans, N.; Zakeeruddin, S. M.; Humphry-Baker, R.; Gratzel, M. *J. Phys. Chem. C* **2007**, *111*, 398.


**10.1021/ja800513m CCC: $40.75** 

***Scheme 1.*** Charge Transfer Reactions Taking Place at the Different Interfaces of a DSSC and the Molecular Structure of N719[a]

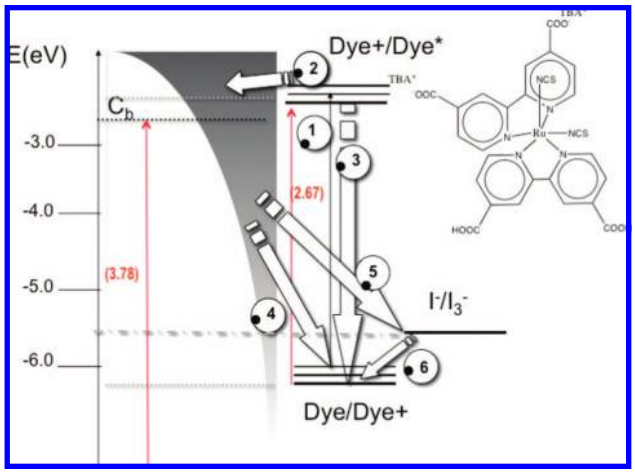


[a] The numbers in parentheses are the energy gap for $TiO_2$ and the N719 dye, and the gray shadow represents the density of electron states. Values in parentheses are the energy versus vacuum level as calculated using ref 13. Reaction 1: light absorption and formation of the dye excited state (solid black arrow). Reaction 2: photoinduced electron injection from the excited dye to the $TiO_2$ conduction band. Reaction 3: luminescence emission from the dye excited state. Reaction 4: electron recombination between photoinjected electrons at $TiO_2$ and the oxidized dye. Reaction 5: electron recombination between photoinjected electrons at $TiO_2$ and the oxidized electrolyte. Reaction 6: dye ground-state regeneration by the electrolyte.

Several authors have studied the different causes that affect the $V_{oc}$ of the DSSC.[14−22] Most of the results are based on the well-established knowledge of the Nernstian behavior[23−27] of the $TiO_2$ semiconductor in the presence of surface dipoles. For example, the use of *tert*-butylpyridine, a base, provokes a positive shift of the $TiO_2$ conduction band and, therefore, an increase in the cell open circuit voltage.[28−30] On the contrary, the presence of acid dipoles has the inverse effect. Moreover, using conformal coatings on the surface of the nanocrystalline $TiO_2$ particles with different basic or acidic metal oxides also influences the cell voltage[31,32] and, thus, the overall device efficiency. Furthermore, systematic work has been carried out on controlling the number of protons in the dye molecules to tune the photocurrent and the voltage of the cell too, and, for example, the mentioned N179 has its more acidic version, with four protons, named N3, that shows upon illumination at a higher photocurrent but a lower $V_{oc}$.[33] Only recently, it has been demonstrated that several dyes, which show poor light-to-energy conversion performance, when employed as sensitizers in a DSSC, do increase the rate of electron recombination between the photoinjected electrons and the oxidized electrolyte, affecting not only the photocurrent but also the cell voltage.[34] As a matter of fact, the molecular structures of those dyes have in common the presence of extended $\pi$-conjugated systems which lie close to the nanoparticle metal oxide surface when anchored.[35] Several authors have previously studied either homoleptic or heteroleptic phenanthroline-based ruthenium(II) complexes and have observed modest light-to-electricity conversion efficiencies when compared to those of devices made using N719 as a sensitizer although the generated photocurrent was comparable to that of the devices made using N719.[36−45] Several hypotheses have been proposed, which are mainly related to a shift of the energy levels of the dye LUMO (lowest unoccupied molecular orbital) or the HOMO (high occupied molecular orbital) due to the introduction of a lower energy $\pi^*$ molecular orbital and, therefore, inefficient photoinduced electron transfer from the dye excited state to the semiconductor conduction band (Scheme 1, reaction 2) or inefficient regeneration of the dye ground state by the electrolyte, respectively, or both (Scheme 1, reaction 6).[38,40] However, there is still an ongoing discussion about the influence of those extended $\pi$-conjugated systems on the interfacial electron transfer reactions at the device. For example, Arakawa and co-workers observed in Ru(II) complexes bearing 4,4′-dicarboxy-2,2′-biquinoline ligands an increase in the dark

(15) Zhang, Z. P.; Zakeeruddin, S. M.; O'Regan, B. C.; Humphry-Baker, R.; Gratzel, M. *J. Phys. Chem. B* **2005**, *109*, 21818.
(16) Kopidakis, N.; Neale, N. R.; Frank, A. J. *J. Phys. Chem. B* **2006**, *110*, 12485.
(17) Kusama, H.; Arakawa, H. *J. Photochem. Photobiol., A* **2003**, *160*, 171–179.
(18) Kusama, H.; Arakawa, H. *J. Photochem. Photobiol., A* **2004**, *165*, 157–163.
(19) Kusama, H.; Arakawa, H. *J. Photochem. Photobiol., A* **2004**, *164*, 103–110.
(20) Kusama, H.; Arakawa, H. *J. Photochem. Photobiol., A* **2004**, *162*, 441–448.
(21) Kusama, H.; Kurashige, M.; Arakawa, H. *J. Photochem. Photobiol., A* **2005**, *169*, 169–176.
(22) Neale, N. R.; Kopidakis, N.; van de Lagemaat, J.; Gratzel, M.; Frank, A. J. *J. Phys. Chem. B* **2005**, 109.
(23) Huang, S. Y.; Schlichthörl, G.; Nozik, A. J.; Grätzel, M.; Frank, A. J. *J. Phys. Chem. B* **1997**, *101*, 2576.
(24) Nozik, A. J. *Annu. Rev. Phys. Chem.* **1978**, *29*, 189.
(25) Yan, S.; Hupp, J. T. *J. Phys. Chem. B* **1996**, *100*, 6867.
(26) Watanabe, T.; Fujishima, A.; Tatsuoki, O.; Honda, K. *Bull. Chem. Soc. Jpn.* **1976**, *49*, 8.
(27) Gerisher, H. *Electrochim. Acta* **1989**, *34*, 1005.
(28) Hara, K.; Dan-Oh, Y.; Kasada, C.; Ohga, Y.; Shinpo, A.; Suga, S.; Sayama, K.; Arakawa, H. *Langmuir* **2004**, *20*, 4205.
(29) Huang, S. Y.; Schlichthoerl, G.; Nozik, A. J.; Graetzel, M.; Frank, A. J. *J. Phys. Chem. B* **1997**, *101*, 2576–2582.
(30) Yin, X.; Zhao, H.; Chen, L.; Tan, W.; Zhang, J.; Weng, Y.; Shuai, Z.; Xiao, X.; Zhou, X.; Li, X.; Lin, Y. *Surf. Interface Anal.* **2007**, *39*, 809–816.
(31) Bandaranayake, K. M. P.; Indika Senevirathna, M. K.; Prasad Weligamuwa, P. M. G. M.; Tennakone, K. *Coord. Chem. Rev.* **2004**, *248*, 1277–1281.
(32) Diamant, Y.; Chappel, S.; Chen, S. G.; Melamed, O.; Zaban, A. *Coord. Chem. Rev.* **2004**, *248*, 1271–1276.
(33) Nazzeruddin, M. K.; Zakeeruddin, S. M.; Humphry-Baker, R.; Jirousek, M.; Liska, P.; Vlachopolous, N.; Shklover, V.; Fisher, C. H.; Grätzel, M. *Inorg. Chem.* **1999**, *38*, 6298.
(34) O'Regan, B. C.; Lopez-Duarte, I.; Martínez-Díaz, M.; Forneli, A.; Albero, J.; Morandeira, A.; Palomares, E.; Torres, T.; Durrant, J. R. *J. Am. Chem. Soc.* **2008**, *130*, 2906.
(35) Palomares, E.; Martínez-Díaz, M. V.; Haque, S.; Torres, T.; Durrant, J. R. *Chem. Commun.* **2004**, 2112.
(36) Hara, K.; Horiuchi, H.; Katoh, R.; Pratap Singh, L.; Sugihara, H.; Sayama, K.; Murata, S.; Tachiya, M.; Arakawa, H. *J. Phys. Chem. B* **2002**, *106*, 374.
(37) Hara, K.; Sugihara, H.; Pratap Singh, L.; Islam, A.; Katoh, R.; Yanagida, M.; Sayama, K.; Murata, S.; Arakawa, H. *J. Photochem. Photobiol., A* **2001**, *145*, 117.
(38) Hara, K.; Sugihara, H.; Tachibana, Y.; Islam, A.; Yanagida, M.; Sayama, K.; Arakawa, H. *Langmuir* **2001**, *17*, 5992.
(39) Islam, A.; Sugihara, H.; Arakawa, H. *J. Photochem. Photobiol., A* **2003**, *158*, 131.
(40) Kukrek, A.; Wang, D.; Hou, Y.; Zong, R.; Thummel, R. *Inorg. Chem.* **2006**, *45*, 10131.
(41) Onozawa-Komatsuzaki, N.; Kitao, O.; Yanagida, M.; Himeda, Y.; Sugihara, H.; Kasuga, K. *New J. Chem.* **2006**, *30*, 689.
(42) Schwarz, O.; van Loyen, D.; Jockusch, S.; Turro, N. J.; Dürr, H. *J. Photochem. Photobiol., A* **2000**, *132*, 91.
(43) Yanagida, M.; Miyamoto, K.; Sayama, K.; Kasuga, K.; Kurashige, M.; Abe, Y.; Sugihara, H. *J. Phys. Chem. C* **2007**, *111*, 201.
(44) Yanagida, M.; Pratap Singh, L.; Sayama, K.; Hara, K.; Katoh, R.; Islam, A.; Sugihara, H.; Arakawa, H.; Nazeeruddin, M. K.; Gratzel, M. *J. Chem. Soc., Dalton Trans.* **2000**, 2817.
(45) Yanagida, M.; Yanaguchi, T.; Kurashige, M.; Hara, K.; Katoh, R.; Sugihara, H.; Arakawa, H. *Inorg. Chem.* **2003**, *42*, 7921.

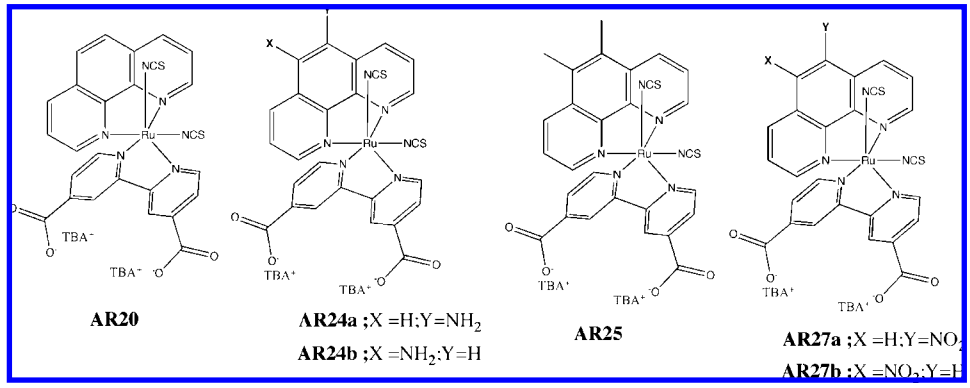


***Figure 1.*** Molecular structures for the Ru(II) complexes utilized in the present study.

current ($e^-$−$TiO_2$/electrolyte$^+$) (Scheme 1, reaction 5) when compared to that of the standard N719 DSSC.[39,45] Moreover, Thummel et al. have recently reported the synthesis of new homoleptic 1,8-naphthyridine-based Ru(II) complexes that show modest incident photon-to-current efficiencies (IPCEs), and they have assigned those results to the low yield of photoinduced electron injection of the complexes into the semiconductor.[40] Furthermore, it has been postulated that some organic dyes based on thiophene groups show a clear dependence between their structure and the $V_{oc}$; increasing the number or thiophene bridge units on the organic dye increases drastically the dark current.[46,47] Hence, it seems there is a general trend between extending the $\pi$-conjugated ligand and the cell voltage.

Taking into account all these observations mentioned above, we have designed a series of heteroleptic ruthenium(II) complexes where one of the 4,4′-dicarboxy-2,2′-bipyridine ligands has been substituted by a phenanthroline moiety (Figure 1) with the aim to achieve high photocurrents and study the effect of the dye molecular structure on the cell voltage. Moreover, the phenanthroline ligand has been modified with the introduction of electron-donating or electron-withdrawing groups to achieve the desired control over the molecular orbitals. While electron-donating groups should decrease the energy gap (HOMO−LUMO gap), the introduction of electron-withdrawing groups should have the opposite effect, and thus, we expect a variation in the DSSC performance.

## Experimental Section

**Synthesis and Characterization of Ru(II) Complexes.** The syntheses of all complexes were carried out following the procedure in a previous paper published in the literature by Kasuga et al.[41] All the chemical products were purchased from Sigma-Aldrich and used without further purification if not otherwise stated.

**1. Synthesis of *cis*-(4,4′-Dicarboxy-2,2′-bipyridine)(1,10-phenanthroline)(dithiocyanate)ruthenium(II) ([Ru(dcbpy)(phen)(NCS)$_2$]) (AR20).** The AR20 complex was already synthesized and characterized by Kasuga et al.[41] Dichloro(*p*-cymene)ruthenium(II) (120 mg, 0.2 mmol) was dissolved in 30 mL of dimethylformamide in a three-necked round bottomed flask completely covered with aluminum foil. The flask was purged with argon for 15 min. 1,10-Phenanthroline (70.6 mg, 0.4 mmol) was added with stirring. The reaction mixture was heated at 60 °C for 4 h. After this time 4,4′-dicarboxy-2,2′-bipyridine (95.62 mg, 0.4 mmol) was added, and the reaction mixture was heated at 160 °C for 4 h under argon and in the absence of light to avoid cis to trans isomerization. Then ammonium thiocyanate (0.99 g, 13 mmol) was added, and the reaction mixture was maintained at 150 °C for 5 h. After the reaction crude was kept cool at room temperature, the solvent was removed under vacuum. Then 5 mL of Milli-Q water was added to remove the ammonium thiocyanate excess. A brown precipitate appeared, and it was collected by filtration with a sintered glass crucible. The product was washed three times with water and diethyl ether. The reaction crude was purified by size exclusion chromatography. The product was dissolved in a mixture of 2.5 mL of methanol and 0.5 mL of tetrabutylammonium hydroxide (40% by weight) to form the tetrabutylammonium salt of the ruthenium complex. This solution was purified using an LH-20 Sephadex column (2.5 × 30 cm) using methanol as the mobile phase. The main red band was collected, and the solvent was evaporated under vacuum. A few drops of 0.01 M $HNO_3$ was added to the resulting semisolid product until a brown precipitate appeared. It was collected with a sintered glass crucible and dried under vacuum. Yield: 81.5%. $^1$H NMR (400 MHz, DMF-$d_7$): $\delta$ 9.94 (d, $J$ = 5.8 Hz, 1H), 9.92 (d, $J$ = 5.3 Hz, 1H), 9.43 (s, 1H), 9.24 (s, 1H), 9.15 (d, $J$ = 8.3 Hz, 1H), 8.78 (d, $J$ = 8.3 Hz, 1H), 8.63 (d, $J$ = 5.8 Hz, 1H), 8.61 (d, $J$ = 8.8 Hz, 1H), 8.56 (dd, $J$ = 8.3, 5.3 Hz, 1H), 8.49 (d, $J$ = 8.8 Hz, 1H), 8.38 (d, $J$ = 5.3 Hz, 1H), 8.14 (d, $J$ = 5.9 Hz, 1H), 7.85 (dd, $J$ = 8.3, 5.3 Hz, 1H), 7.75 (d, $J$ = 5.9 Hz, 1H). ESIMS: $m/z$ 643 (M + H).

**2. Synthesis of *cis*-(4,4′-Dicarboxy-2,2′-bipyridine)(5-amino-1,10-phenanthroline)(dithiocyanate)ruthenium(II)[Ru(dcbpy)-(aphen)(NCS)$_2$] (AR24).** The synthesis of AR24 was carried out following a procedure like that of compound AR20 except that 5-amino-1,10-phenanthroline (83 mg, 0.4 mmol) was added instead of 1,10-phenanthroline. The solid obtained was analyzed by $^1$H and COSY NMR spectroscopy, and two diastereoisomers were observed in a 1:1 proportion. Yield: 54.6%. The different products were separated by reversed-phase $C_{18}$ semipreparative HPLC, using a mixture of $H_2O$ (0.1% TFA (trifluoroacetic acid))/MeCN (0.1% TFA) (73:23) as the mobile phase. Two compounds were isolated with a retention time of 16.36 and 18.8 min, respectively, and finally, the solvent was removed under vacuum. Yield: 46.67%.

The following are data for compound AR24a ($t_R$ = 16.36 min). $^1$H NMR (400 MHz, MeOD): $\delta$ 9.72 (d, $J$ = 5.3 Hz, 1H), 9.56 (d, $J$ = 5.9 Hz, 1H), 9.00 (s, 1H), 8.91 (d, $J$ = 8.6 Hz, 1H), 8.81 (s, 1H), 8.22 (d, $J$ = 5.7 Hz, 1H), 8.14 (dd, $J$ = 8.6, 5.3 Hz, 1H), 7.97 (d, $J$ = 8.3 Hz, 1H), 7.46 (d, $J$ = 5.3 Hz, 1H), 7.45 (m, 2H), 7.29 (dd, $J$ = 8.3, 5.3 Hz, 1H), 7.07 (s, 1H). ESIMS: $m/z$ 658 (M + H).

The following are data for compound AR24b ($t_R$ = 18.8 min). $^1$H NMR (400 MHz, MeOD): $\delta$ 9.74 (d, $J$ = 5.6 Hz, 1H), 9.32 (d, $J$ = 5.1 Hz, 1H), 9.01 (s, 1H), 8.88 (s, 1H), 8.54 (d, $J$ = 8.5 Hz, 1H), 8.32 (d, $J$ = 5.6 Hz, 1H), 8.31 (d, $J$ = 8.3 Hz, 1H), 7.92 (dd, $J$ = 8.3 5.1 Hz, 1H), 7.86 (d, $J$ = 5.2 Hz, 1H), 7.71 (d, $J$ = 5.9 Hz, 1H), 7.54 (d, $J$ = 5.9 Hz, 1H), 7.45 (dd, $J$ = 8.5, 5.3 Hz, 1H), 7.15 (s, 1H). ESIMS: $m/z$ 658 (M + H).

(46) Hara, K.; Miyamoto, K.; Abe, Y.; Yanagida, M. *J. Phys. Chem. B* **2005**, *109*, 23776.
(47) Hara, K.; Sato, T.; Katoh, R.; Furube, A.; Ohga, Y.; Shinpo, A.; S., S.; Sayama, K.; Sugihara, H.; Arakawa, H. *J. Phys. Chem. B* **2003**, *107*, 597.

**3. Synthesis of *cis*-(4,4′-Dicarboxy-2,2′-bipyridine)(5,6-dimethyl-1,10-phenanthroline)(dithiocyanate)ruthenium(II) [Ru(dcbpy)(dmphen)$(NCS)_2$] (AR25).** The synthesis of AR25 was carried out following the procedure as detailed for the synthesis of compound AR20, adding 5,6-dimethyl-1,10-phenanthroline (81.6 mg, 0.4 mmol) instead of 1,10-phenanthroline. Yield: 56.6%. $^1$H NMR (400 MHz, DMF-$d_7$): $\delta$ 9.75 (d, $J$ = 5.8 Hz, 1H), 9.68 (d, $J$ = 5.3 Hz, 1H), 9.26 (d, 1H), 9.06 (d, 1H), 9.04 (d, $J$ = 8.5 Hz, 1H), 8.66 (d, $J$ = 8.5 Hz, 1H), 8.44 (dd, $J$ = 5.8 Hz, 1H), 8.35 (dd, $J$ = 8.5, 5.3 Hz, 1H), 8.11 (d, $J$ = 5.3 Hz, 1H), 7.92 (d, $J$ = 5.9 Hz, 1H), 7.63 (dd, $J$ = 8.5, 5.3 Hz, 1H), 7.56 (dd, $J$ = 5.9, Hz, 1H), 2.92 (s, 3H), 2.81 (s, 3H). ESIMS: $m/z$ 670 (M + H).

**4. Synthesis of *cis*-(4,4′-Dicarboxy-2,2′-bipyridine)(5-nitro-1,10-phenanthroline)(dithiocyanate)ruthenium(II) [Ru(dcbpy)(nophen)$(NCS)_2$] (AR27).** The synthesis of AR27 was carried out following the procedure as detailed for the synthesis of compound AR20, adding 5-nitro-1,10-phenanthroline (81.6 mg, 0.4 mmol) instead of 1,10-phenanthroline. Two stereoisomers were observed by proton and COSY NMR experiments in a 1:1 proportion. Yield: 62%. The products were separated by $C_{18}$ reversed-phase semipreparative HPLC, using MeCN (0.1% TFA)/$H_2O$ (0.1% TFA) (70:30) as the eluent. Two compounds were isolated with a retention time of 16.03 and 18.47 min, respectively. Yield: 55.8%.

The following are data for compound AR27a ($t_R$ = 16.03 min). $^1$H NMR (400 MHz, MeOD) $\delta$ 9.15 (dd, $J$ = 5.6 Hz, 1H), 8.96 (d, $J$ = 5.8 Hz, 1H), 8.86 (s, 1H), 8.59 (s, 1H), 8.56 (dd, $J$ = 8.3 Hz, 1H), 8.41 (s, 1H), 8.33 (dd, $J$ = 8.6 Hz, 1H), 7.90 (dd, $J$ = 8.3, 5.4 Hz, 1H), 7.81 (d, $J$ = 5.4 Hz, 1H), 7.54 (d, $J$ = 5.3 Hz, 1H), 7.19 (d, $J$ = 5.8 Hz, 1H), 7.17 (dd, $J$ = 8.6, 5.3 Hz, 1H), 6.91 (d, $J$ = 5.6 Hz, 1H). ESIMS: $m/z$ 688 (M + H).

The following are data for compound AR27b ($t_R$ = 18.47 min). $^1$H NMR (400 MHz, MeOD): $\delta$ 9.34 (dd, $J$ = 5.4, Hz, 1H), 9.17 (d, $J$ = 5.8 Hz, 1H), 8.80 (d, $J$ = 8.7 Hz, 1H), 8.71 (s, 1H), 8.60 (s, 1H), 8.41 (s, 1H), 8.15 (d, $J$ = 8.2 Hz, 1H), 7.91 (dd, $J$ = 8.7, 5.3 Hz, 1H), 7.87 (d, $J$ = 5.8 Hz, 1H), 7.62 (dd, $J$ = 5.3, Hz, 1H), 7.26 (d, $J$ = 5.9 Hz, 1H), 7.14 (dd, $J$ = 8.2, 5.4 Hz, 1H), 6.99 (dd, $J$ = 5.9 Hz, 1H). ESIMS: $m/z$ 688 (M + H).

**Optical, Electrochemical, and Spectroscopic Measurements.** The UV−vis and fluorescence spectra were recorded using a 1 cm path length quartz cell on a Shimadzu UV spectrophotometer 1700 and an Aminco-Bowman series 2 luminescence spectrometer with a temperature controller, respectively.

The electrochemical data were obtained employing a conventional three-electrode cell connected to a CH Instruments 660c potentiostat−galvanostat. For cyclic voltammetry, we used a platinum working electrode, a calomel reference electrode (saturated calomel electrode, SCE), and a platinum wire as the auxiliary electrode. The picosecond to microsecond emission lifetime measurements were carried out with a Lifespec picosecond fluorescence lifetime spectrometer from Edinburgh Instruments. As excitation sources two diode lasers, with 405 and 635 nm nominal wavelengths, were used. The instrument response measured at the FWHM (full-width at half-maximum) was below 350 ps. Laser transient absorption spectroscopy (L-TAS) measurements were carried out with a home-built system as reported before.[35]

Charge extraction and photovoltage measurements were carried out using a home-built system. In brief, the charge extraction data were acquired using a pulse generated by an array of white LEDs. The decay was monitored using a Tektronics oscilloscope TDS 2022 and recorded using the Tektronics data acquisition software. We applied different light intensities to achieve different open circuit voltages of the cell, and immediately after the light pulse the device was short-circuited to extract the charge, which was controlled with a switch. For the photovoltage transients, the pulse was generated with red-emitting diodes while the cell was illuminated with the same array of white light diodes.

Proton NMR spectra, NOESY and COSY experiments, were measured on a Bruker 400 MHz spectrometer. A Waters LCT Premier liquid chromatograph coupled with a time-of-flight mass spectrometer with electrospray ionization (ESI) was used to measure the mass spectra.

**Nanoparticle Synthesis and Film Preparation.** The nanocrystalline $TiO_2$ particles were synthesized as reported before.[48] In brief, titanium isopropoxide (40 mL, 0.13 mol) was added to glacial acetic acid (9.12 g) under an argon atmosphere with stirring. The reaction mixture was cooled in an ice bath, and 0.1 M nitric acid (240 mL) was added with vigorous stirring. The mixture was heated in an oil bath at 80 °C for 8 h and, after cooling, was filtered through a 0.45 $\mu$m syringe filter. The resulting product was diluted to 5% by weight of $TiO_2$ by adding water and then was autoclaved at 220 °C for 12 h. The aqueous phase was removed by centrifugation, and the solid nanoparticles were isolated and rinsed twice with ethanol. An ultrasonic horn was used to break the aggregates, and the solvent was removed under vacuum. The solid nanoparticles were diluted to 15% by $TiO_2$ weight, using ethyl cellulose and terpineol, and the paste was homogenized by ball milling.

The $Al_2O_3$ mesoporous films were synthesized using commercially available $Al_2O_3$ nanoparticles.

**Device Preparation and Characterization.** In the present work we have utilized two different types of devices due to their characterization. Highly transparent thin film devices were utilized for time-correlated single photon counting (TCSPC) and L-TAS experiments. These devices were made using 4 $\mu$m thick films and sensitized with the ruthenium complexes until the absorbance at the metal-to-ligand charge transfer (MLCT) band of the sensitized film was 0.6 absorption unit. On the other hand, for optimized efficiencies all the devices studied during this work were made using 16 $\mu$m thick films consisting of a layer of 12 $\mu$m of 19 nm $TiO_2$ nanoparticles and a layer of 4 $\mu$m of 300 nm $TiO_2$ nanoparticles (scatter layer). In both cases, the films were deposited onto a conducting glass substrate (Hafford Glass Inc., with 15 $\Omega/cm^2$ resistance) using the well-known doctor blade technique. For the thin film devices the area was 1 $cm^2$, while in the case of the thick film DSSC the active area was 0.152 $cm^2$. The counter electrodes were made by spreading a solution of $H_2PtCl_6$ in ethanol onto a conducting glass substrate with a small hole to allow the introduction of the liquid electrolyte using a vacuum. Two liquid electrolytes were used depending on the measurements; AF19 is composed of 0.6 M DMPII (1-propyl-2,3-dimethylimidazolium iodide), 0.04 M $I_2$, and 0.025 M LiI in acetonitrile/valeronitrile (85:15), and AF4 was made using 0.6 M DMPII (1-butyl-3-methylimidazolium iodide), 0.04 M $I_2$, 0.025 M LiI (guanidinium isothiocyanate), and 0.28 M *tert*-butylpyridine in acetonitrile/valeronitrile (85:15). The photovoltaic measurements were carried out with a 150 W xenon lamp from Oriel Instruments with the appropriate set of filters for the correct simulation of the 1.5 AM G solar spectrum. The incident light power was calibrated using a silicon photodiode previously calibrated at 1000 $W/m^2$ at 1.5 AM G.

**Theoretical Calculations.** The geometries of the different complexes were calculated with Gaussian 03, revision C.02,[49] using the B3LYP functional. 6-31G(d) basis sets were used for sulfur, oxygen, nitrogen, carbon, and hydrogen atoms, whereas the Stuttgart−Dresden effective core potential (ECP)[50] and corresponding basis set were used for ruthenium. HOMO and LUMO orbitals were calculated from the optimized geometries.

## Results and Discussion

**Spectroscopic Properties. 1. UV−Vis Absorption Spectra and Photoluminescence Measurements.** Figure 2 illustrates the UV−vis spectra of AR20, AR24, AR25, AR27, and N719 in dimethylformamide (DMF). The absorption band in the visible

(48) Palomares, E.; Vilar, R.; Green, A.; Durrant, J. R. *Adv. Funct. Mater.* **2004**, *14*, 111.
(49) Frisch, M. J.; et al. *Gaussian 03*, Revision C.02; Gaussian, Inc.: Wallingford, CT, 2004.
(50) Andrae, D.; Häusserman, U.; Dolg, M.; Stoll, H.; Preuss, H. *Theor. Chim. Acta* **1990**, *77*, 123.

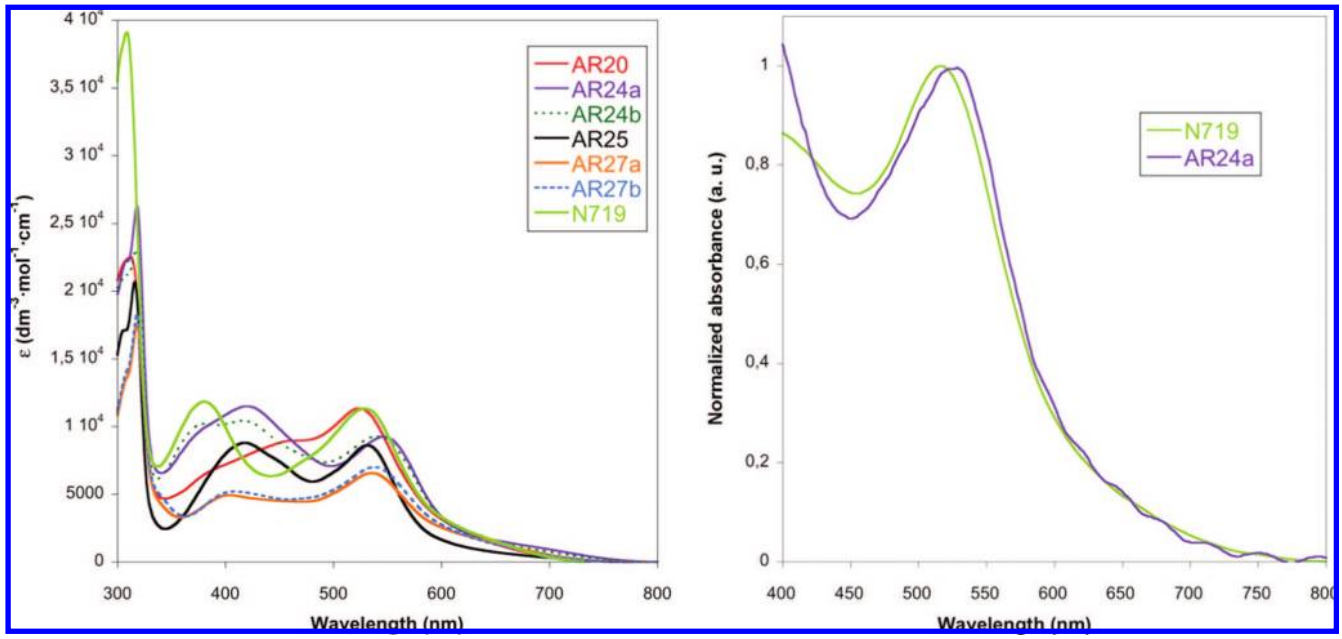


***Figure 2.*** UV−vis absorption spectra of all the Ru(II) complexes described above in DMF (left) and adsorbed on a 4 $\mu$m thick $TiO_2$ transparent mesoporous film (right). The sensitization was 30 min at 50 °C (the concentration of the dye solution was $1 \times 10^{-4}$ M).

***Table 1.*** UV−Vis Absorption Parameters (nm) for the Ruthenium(II) Complexes Described Above

| ruthenium complex | $\pi-\pi^*$ | MLCT |
|---|---|---|
| AR20 | 415 (7830)[a] | 522 (11360) |
| AR24a | 420 (11500) | 546 (9242) |
| AR24b | 415 (10441) | 545 (9312) |
| AR25 | 415 (8820) | 531(8606) |
| AR27a | 403 (5220) | 538 (6984) |
| AR27b | 400 (4938) | 535 (6560) |
| N719 | 378 (11852) | 527 (11360) |

[a] The numbers in parentheses correspond to the molecular extinction coefficient ($dm^3\ mol^{-1}\ cm^{-1}$).

region has been previously assigned to the MLCT in ruthenium(II) complexes.[51] Table 1 shows the most important parameters for all the ruthenium complexes. As can be observed, in the case of AR24 and AR27 the amino and the nitro groups on the phenanthroline induce a red shift of the maximum. It is worth noting that the visible spectra of the dyes adsorbed onto $TiO_2$ transparent thin mesoporous films retain the red shift as in solution (Figure 2, right). However, we note that the lower energy of the visible transition for the AR24 dye appears to be in contradiction to the expected increase in the optical gap.[52]

The photoluminescence properties of the dyes in solution and adsorbed onto transparent mesoporous thin films have also been measured. The emission of the dye-sensitized films is dramatically quenched for the $TiO_2$ samples when compared to that of $Al_2O_3$-sensitized films, which, in principle, suggests the existence of efficient light-induced electron injection from the dye excited state into the $TiO_2$ semiconductor conduction band (CB). Absorption of the dye to an oxide surface could in principle reduce the emission without the presence of electron injection. For this reason it is better to compare the luminescence of the dye on $TiO_2$ to the luminescence on another substrate such as $Al_2O_3$, where the conduction band edge is above the LUMO of the molecule. The results indicate that dye-sensitized $Al_2O_3$ films

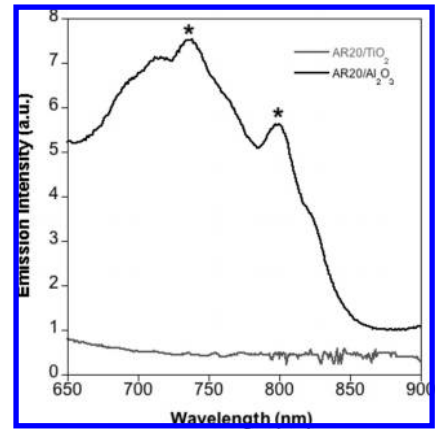


***Figure 3.*** Photoluminescence spectra of AR20-sensitized films recorded under normal conditions ($\lambda_{ex}$ = 500 nm). The asterisks indicate optical artifacts from the luminescence spectrophotometer.

show typical photoluminescence at room temperature when excited at the MLCT band as in solution.

Figure 3 illustrates, as an example, the AR20/$Al_2O_3$ emission spectra, and the most relevant photoluminescence properties for all dyes are listed in Table 2. In the case of AR27 we were only able to measure the emission kinetics in solution since we could not resolve the decay on either $TiO_2$ or $Al_2O_3$ as it was faster than our instrument response. This observation can be understood, if we take into account that the AR27 complex fulfills the band gap law. In brief, the smaller the energy gap, the lower the complex emission quantum yield and the faster its emission decay dynamics.

To determine the photoinduced electron transfer yield of those dyes into $TiO_2$, we have carried out further experiments to study the dyes in complete devices. It has been previously shown that TCSPC is a convenient technique that can be used to estimate not only the yield of the electron injection in a qualitative way,

(51) Lakowicz, J. R. *Principles of Fluorescence Spectroscopy*, 2nd ed.; Kluwer Academic/Plenum Publishers: New York, 1999.

(52) Hou, Y.; Xie, P.; Wu, K.; Wang, J.; Zhang, B.; Cao, Y. *Solar Energy Mater. Solar Cells* **2001**, *70*, 131–139.

***Table 2.*** Photophysical Parameters for the Ruthenium(II) Complexes Described above in DMF Solution[a]

| complex | emission ($\lambda_{max}$, nm) | $E_{0-0}$[b] (eV) | solution lifetime (ns) | $Al_2O_3$ film emission lifetime[d] (ns) | DSSC emission lifetime (ns) | estimated electron injection yield (%) |
|---|---|---|---|---|---|---|
| AR20 | 724 | 1.93 | 3.82 (3) | 11.90 (10) | 1.44 (40.3) | ~85 |
| | | | 51.92 (97) | 34.49 (90) | 7.70 (56.7) | |
| AR24a | 777 | 1.89 | 10.05 (33.2) | 11.16 (40.2) | 2.34 (50.6) | ~70 |
| | | | 47.65 (66.8) | 36.86 (59.8)) | 12.53 (49.4) | |
| Ar24b | 774 | 1.9 | 11.03 (38.3) | 11.56 (43.2) | 2.51 (41.6) | ~70 |
| | | | 54.03 (61.6) | 32.97 (56.8) | 20.98 (58.4) | |
| AR25 | 746 | 1.92 | 9.57 (18.9) | 11.96 (20.6) | 2.23 (48.5) | ~90 |
| | | | 56.67 (81.1) | 37.36 (79,4) | 12.61 (51.5) | |
| AR27a | 760 | 1.52[c] | 3.41 (7.76) | | | |
| | | | 12.8 (92.2) | | | |
| | 760 | 1.53[c] | 1.57 (6.30) | | | |
| AR27b | | | 12.95 (93.70) | | | |

[a] The numbers in parentheses are the percentage for each parameter. [b] The 0−0 energy was calculated using the tangent from the higher energy side of the emission band except for AR27. [c] Estimated from the electrochemical data. [d] The emission lifetime for the AR27 complex is shorter than the instrument response of our TCSPC system (IR = 350 ps).

but also the rate of electron injection dynamics in the DSSC.[53,54] However, it is necessary, as a control, to determine the native excited lifetime ($\tau$) of the molecules adsorbed onto the nanoparticle surface. Thus, as explained before, we employed $Al_2O_3$ mesoporous sensitized films as a control.

As detailed in Table 2, in the absence of electrolyte, either in solution or adsorbed onto $Al_2O_3$ thin films, the emission kinetics were fitted to a biexponential decay, and a slow component was observed in all decays. Several authors have reported that the slow component of the dye excited lifetime decay arises from the nature of the dye's triplet excited state.[51,55] More interesting is the difference in emission decay amplitude when the dye-sensitized $Al_2O_3$ films are compared with the photovoltaic devices. For a fixed acquisition time of 900 s we can observe (Figure 4) faster emission decay kinetics for complete devices and a decrease in the signal amplitude and the area under the curve. In fact, we evaluate the electron injection yield by comparison of the decay curves between both sets of samples ($Al_2O_3$ vs DSSC). As can be observed in Figure 4, in all cases the photoinduced electron injection is efficient, and in the case of AR25, the yield is near 90%. Those values are similar to those previously reported for N719. Furthermore, using the same mathematical procedure as published by Koops et al.,[53] we have estimated that the photoinduced electron injection reaction takes place faster than in 175 ps, which is in good agreement with previously published data for ruthenium(II) complexes used in a complete DSSC.[56,57]

**2. L-TAS and Electrochemical Measurements.** Transient absorbance measurements were performed either on dye-sensitized 4 $\mu$m thick transparent mesoporous $TiO_2$ or in complete functional devices and are shown in Figures 5 and 6. Consistent with previous reports, we associated the decay of the dye−$TiO_2$ sample with the photoinduced electron recombination kinetics between the electrons at $TiO_2$ and the oxidized dye at the nanoparticle surface[58−60] (Scheme 1, reaction 4). Moreover, in good agreement with previous papers, the electron recombination kinetics can be fitted to a classic stretched exponential which is consistent with the presence of a large distribution of recombination sites within the mesoporous film with different energetic characteristics. These differences in the local environment not only lead to a variation of the recombination kinetics but also have been observed for the electron injection dynamics.[8−10,59] Back electron transfer half-times ($\tau_{1/2}$), measured at fwhm (full width at half-maximum), for the heteroleptic Ru(II) complexes are summarized in Table 3.

The L-TAS study of complete functional devices (Figure 6) reveals that, in the presence of $I^-/I_3^-$, the amplitude of the initial signal is strongly reduced for AR24 relative to AR25. Note that Figure 3 indicates the same degree of luminescence quenching for both dyes. This indicates that either the photoinduced electron injection is strongly reduced when $I^-/I_3^-$ is present in AR24/DSCC (the same behavior is observed for AR27/DSSC) or the oxidized dye is removed by a very fast recombination with the injected electron, or both. For efficient devices based on homo- or heteroleptic ruthenium(II) complexes, in the presence of redox-active electrolyte the L-TAS recombination dynamics always appears associated with the appearance of long-lived transient decays assigned previously by Montanari et al. to the electrons at $TiO_2$.[34,61] In our case, when we measured the dynamics of AR24/DSSC (Figure 6, $\lambda_{probe} = 1000$ nm), the amplitude of this slow decay component on the L-TAS recombination kinetics was remarkably low. In fact, the comparison of the yield of photoinduced electrons at $TiO_2$ between AR24/DSSC and AR25/DSSC shows that for AR25/DSSC the yield of electrons is 8 times higher than for AR24/DSSC. It seems clear that the differences in the molecular structure of both dyes are playing a major role in the interfacial charge transfer reactions at the devices.

Moreover, these differences cannot be explained in terms of different energy levels of the molecular orbitals since the analysis of the cyclic voltammetry reveals that AR24 and AR25 show almost identical reduction potentials as confirmed by the theoretical study below.

**Computational Study.** We have performed theoretical calculations using the software package Gaussian 03 as described in the Experimental Section. Figure 7 illustrates the graphical representation of the HOMO and LUMO orbitals of the

(53) Koops, S.; Durrant, J. R. *Inorg. Chim. Acta* **2007**, *361*, 663.
(54) Tachibana, Y.; Rubtsov, I. V.; Montanari, I.; Yoshihara, K.; Klug, D. R.; Durrant, J. R. *J. Photochem. Photobiol., A* **2001**, *142*, 215.
(55) Balzani, V.; Scandola, F. *Supramolecular Photochemistry*; Ellis Horwood Ltd.: Chichester, U.K., 1991.
(56) Myahkostupov, M.; Piotrowiak, P.; Wang, D.; Galloppini, E. *J. Phys. Chem. C* **2007**, *111*, 2827.
(57) Myllyperkioe, P.; Benko, G.; Korpi-Tommla, J.; Yartsev, A. P.; Sundstroem, V. *ChemPhysChem* **2008**, *10*, 996.
(58) Guo, J.; She, C.; Lian, T. *J. Phys. Chem. C* **2007**, *111*, 8979.
(59) Hao, E.; Anderson, N. A.; Asbury, J. B.; Lian, T. *J. Phys. Chem. B* **2002**, *106*, 10191.
(60) Palomares, E.; Clifford, J. N.; Lutz, T.; Haque, S.; Durrant, J. R. *J. Am. Chem. Soc.* **2003**, *125*, 475.
(61) Montanari, I.; Nelson, J.; Durrant, J. R. *J. Phys. Chem. B* **2002**, *106*, 12203–12210.

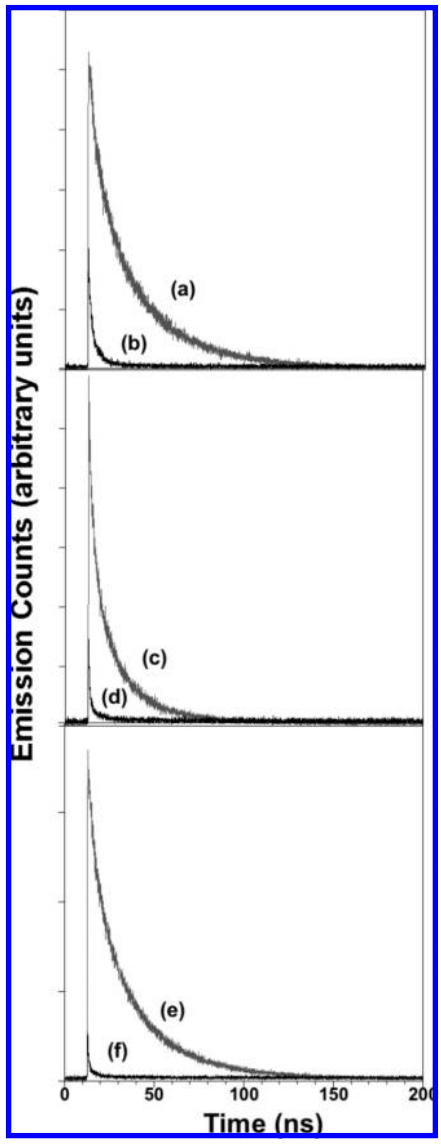


***Figure 4.*** Photoluminescence emission decays for (a) AR20/$Al_2O_3$, (b) AR20/DSSC, (c) AR24/$Al_2O_3$, (d) AR24/DSSC, (e) AR25/$Al_2O_3$, (f) and AR25/DSSC. The decays were recorded upon excitation at $\lambda_{ex} = 405$ nm with monitoring at the maximum emission wavelength ($\lambda_{AR20} = 714$ nm, $\lambda_{AR24} = 775$ nm, and $\lambda_{AR25} = 746$ nm). The electrolyte was AF19.

heteroleptic Ru(II) complexes. In all cases the electrons on the HOMO are centered on the axial thiocyanate ligands and, within those, on the sulfur atoms. On the other hand, the electrons on the LUMO are localized on the bipyridine ligand for the AR20, AR24, and AR25 complexes in good agreement with previous theoretical calculations.[41] In fact, these computational results also support the hypothesis of efficient electron injection in these complexes since the electronic coupling between the 3d Ti orbitals and the LUMO of the Ru(II) complexes must be very strong. However, in the case of the AR27 complex, the electrons on the LUMO orbital are delocalized on the phenanthroline ligand, and thus, this could be one of the reasons for the low device performance.

In fact, we point out that although it was impossible to observe the luminescence dynamics in the case of the AR27/$TiO_2$ or the AR27/$Al_2O_3$ sample, due to the time response of our TCSPC measurement system, the signal at the TAS measurements (Figure 5) reveals that the injection kinetics are not as efficient as for AR20- and AR25-sensitized $TiO_2$ samples.

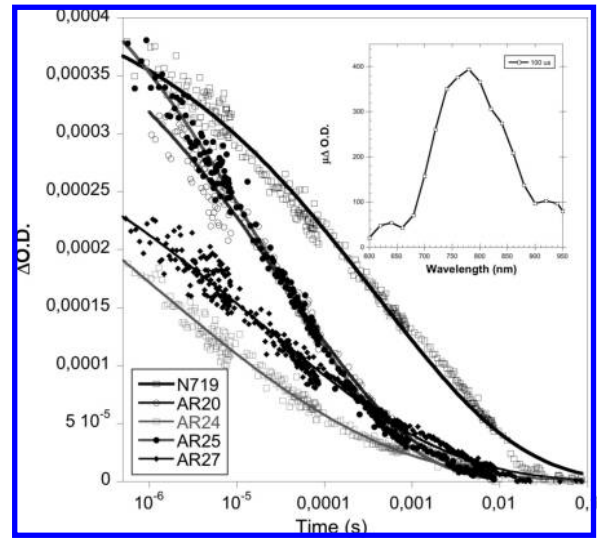


***Figure 5.*** Absorbance transient for 4 $\mu$m thick transparent dye-sensitized $TiO_2$ films ($^{MLCT}\lambda_{abs} = 0.3$). The excitation wavelength was 620 nm, and the probe wavelength was 800 nm. The solid lines correspond to the stretched exponential fit. The inset illustrates the AR20 cation spectra after excitation at 535 nm.

Thus, we can expect a low photocurrent on devices made using AR27. Furthermore, the computational study reveals that the HOMO−LUMO energy gaps for the AR20, AR24, and AR25 dyes show little difference. On the other hand, in the case of the AR27 complex, with the electron-withdrawing nitro group, the HOMO−LUMO energy gap is noticeably smaller. It is worth noting, too, that the theoretical model also predicts small differences between the different AR24 and AR27 diastereoisomers as has been observed in the experimental results. Taking into account that in all cases the binding of the Ru(II) complexes onto the nanoparticles occurs through the bipyridine carboxylic groups, we can assume that the distance between the semiconductor nanoparticle surface and the HOMO orbital for all complexes is almost the same. We have estimated that the distance is about 8 Å. It has been previously reported that, for N719 and other Ru(II) complexes, there is a clear correlation between the HOMO/$TiO_2$ distance and the $e^-$−$TiO_2$/$dye^+$ electron recombination kinetics.[62] In our hands all decay kinetics were faster than those of the standard molecule N719 under the same experimental conditions.

**Photovoltaic Device Characterization.** After the spectroscopic characterization of all the ruthenium(II) complexes described above, we focused on the measurement and analysis of the photoelectrochemical characteristics of the solar cell devices. The IPCE reveals that in the case of devices made using AR20 and AR25 Ru(II) complexes the photon-to-electron conversion efficiency is similar to that reported for N719. However, for the AR24 complex the conversion efficiency is much lower, in good agreement with the low electron injection yield observed in the results above. Nonetheless, the lower photovoltage observed (Table 4) for those cells ($V_{oc} = 0.48$ V) when compared with that of AR20 ($V_{oc} = 0.67$ V) or AR25 ($V_{oc} = 0.67$ V) cells was also surprising. The origin of such an effect on the photovoltage will be discussed in the next section. We focus now on AR27/DSSC; as can be seen in Figure 8 the IPCE

(62) Clifford, J. N.; Palomares, E.; Nazeeruddin, M. K.; Grätzel, M.; Nelson, J.; Li, X.; Long, N. J.; Durrant, J. R. *J. Am. Chem. Soc.* **2004**, *126*, 5225.

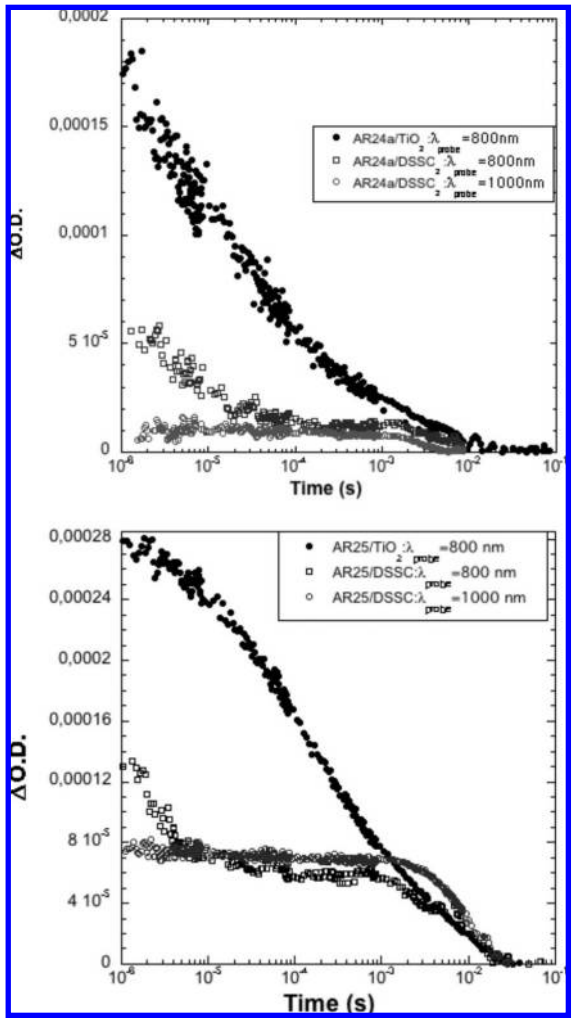


***Figure 6.*** Electron recombination dynamics for a 4 $\mu$m thick transparent film: (top) AR24a/DSSC and (bottom) AR25/DSSC. Both cells have the same absorption ($^{MLCT}\lambda_{abs}$= 0.6). The excitation wavelength was 620 nm. The electrolyte was AF19.

***Table 3.*** Charge Recombination and Electrochemical Potentials for the Heteroleptic Ru(II) Complexes

| sample | half-time recombination decay ($\tau_{1/2}$, ms) | $\alpha^a$ | $E_{1/2}(Ru^{III/II})$ (V) in acetonitrile vs SCE electrode at 25 °C[b] | $E_{1/2}(Ru^{III/II*})$ (V) in acetonitrile vs SCE electrode at 25 °C |
|---|---|---|---|---|
| AR20 | 0.045 | 0.27 | 0.73 | −1.2 |
| AR24a | 0.015 | 0.16 | 0.75 | −1.14 |
| AR24b | 0.015 | 0.16 | 0.75 | −1.15 |
| AR25 | 0.026 | 0.27 | 0.74 | −1.19 |
| AR27a | 0.052 | 0.2 | 0.72 | −0.8 |
| AR27b | 0.052 | 0.2 | 0.72 | −0.81 |
| N719 | 0.44 | 0.26 | 0.73 | −1.2 |

[a] α corresponds to the parameter obtained from the curve fitting of the decay experimental points using the stretched exponential function int ∝ exp[$-(t/\sigma)^{\alpha}$. [b] The solutions (3 mM) were purged with argon for 5 min.

was very low for these devices too. This could be expected from the kinetic measurements and the theoretical calculations that predict a low-lying LUMO level unable to achieve high electron injection yields. On the other hand, the IPCE results for AR24/DSSC cannot be explained like those for AR27, since for AR24 the experimental and the theoretical results predict a high LUMO energy level and, therefore, enough driving force for electron injection onto the $TiO_2$ conduction band. We believe that the

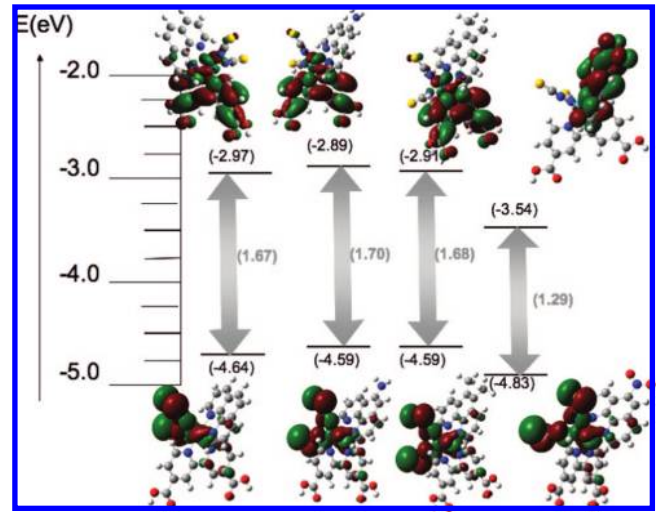


***Figure 7.*** Molecular orbitals and energy gaps of AR20, AR24a, AR25, and AR27a (DFT/6-31H(d), isodensity value 0.02).

***Table 4.*** Device Parameters When Irradiated with Simulated Sunlight (100 mW/cm$^2$, 1.5 AM G)[a]

| cell | $I_{sc}$ (mA) | $V_{oc}$ (V) | FF | $\eta$ (%) |
|---|---|---|---|---|
| AR20 | 1.91 | 0.67 | 46.93 | 3.98 |
| AR25 | 2.05 | 0.67 | 50.20 | 4.56 |
| AR24a | 0.22 | 0.48 | 31.45 | 0.22 |
| AR24b | 0.15 | 0.46 | 30.72 | 0.14 |
| AR27a | 0.8 | 0.44 | 34.21 | 0.8 |
| AR27b | 0.12 | 0.44 | 35.23 | 0.13 |
| N719 | 1.5 | 0.66 | 68.32 | 4.45 |

[a] The cell area was 0.152 cm$^2$ and the electrolyte AF4.

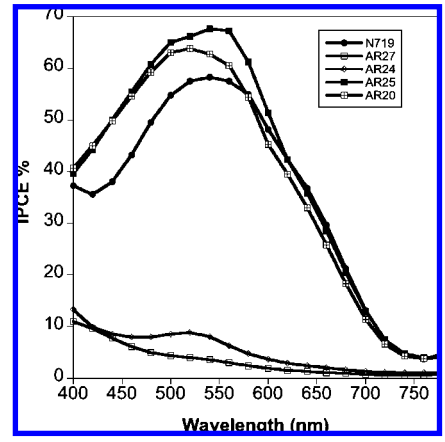


***Figure 8.*** Incident photon-to-current efficiency curves for 12 + 4 $\mu$m thick DSSC using the AF4 electrolyte.

results obtained for AR24/DSSC can be explained either in terms of inefficient electron regeneration from the liquid electrolyte due to an increase in the electron recombination kinetics between the photoinjected electrons and the electrolyte or the low yield of electron injection due to the quenching of the dye excited state by the redox electrolyte. To seek further information on these two hypotheses, we have also studied the photocurrent vs voltage device characteristics of the DSSC under standard illumination conditions (100 mW/cm$^2$). The results are shown in Table 4. We observed that for the solar cells the photocurrent was in good agreement with the measured IPCE.

Moreover, as we mentioned before, it was very interesting to note that the voltage and hence the dark current curves (Figure

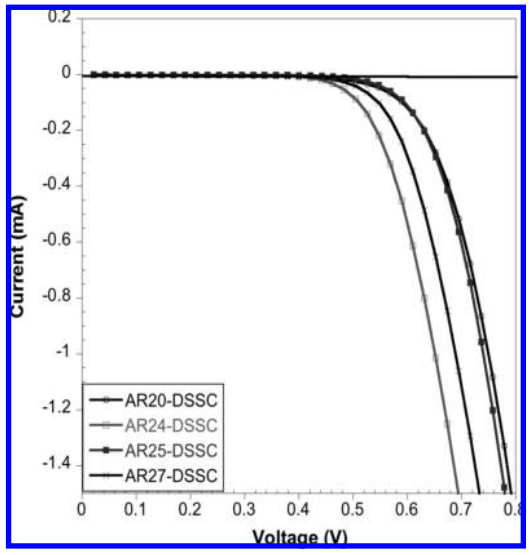


***Figure 9.*** *I*−*V* curves measured for the indicated devices in the dark. The electrolyte was AF19.

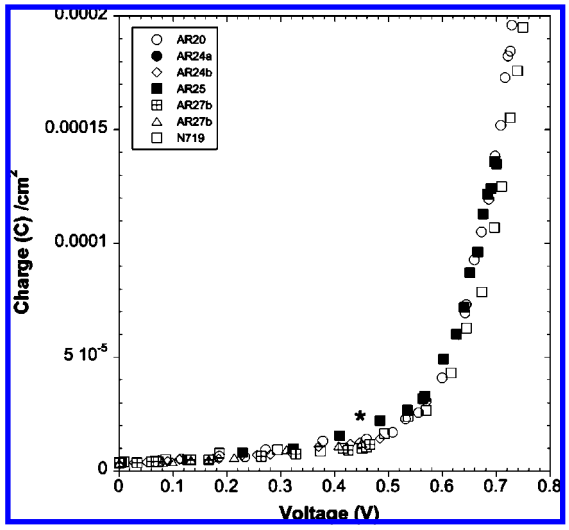


***Figure 10.*** Charge extraction measurements for all devices. The DSSC active area is 1 $cm^2$. The cells were made using a transparent 4 $\mu$m thick $TiO_2$ film sensitized with the Ru(II) complexes and AF19 electrolyte. The asterisk indicates the voltage at which all devices have the same charge.

9) were much different between the different cells despite the fact that all heteroleptic Ru(II) complexes in this study have almost identical energy gaps (except, of course, AR27). Thus, the inefficient performance of these heteroleptic ruthenium dyes must be related to the charge recombination kinetics between the photoinjected electrons and the oxidized redox couple.

For a more detailed study on this issue, we carried out photovoltage transient experiments. Recently, we have employed those measurements, also known as $V_{oc}$ decays, to evaluate the electron recombination dynamics between the photoinjected electrons at $TiO_2$ and the oxidized electrolyte in porphyrin-sensitized solar cells.[63,64] It is worth noting that $V_{oc}$ decays are measurements strongly dependent on the accumulated charge at the semiconductor (charge density), and hence, to obtain a fair comparison of the $e^-$−$TiO_2$/electrolyte$^+$ recombination dynamics between different devices, the charge densities on both cells must be equal. As illustrated in Figure 10, in our case, this condition can be achieved when the cell voltage is 475 mV. As indicated in Table 4 the different solar cells have different

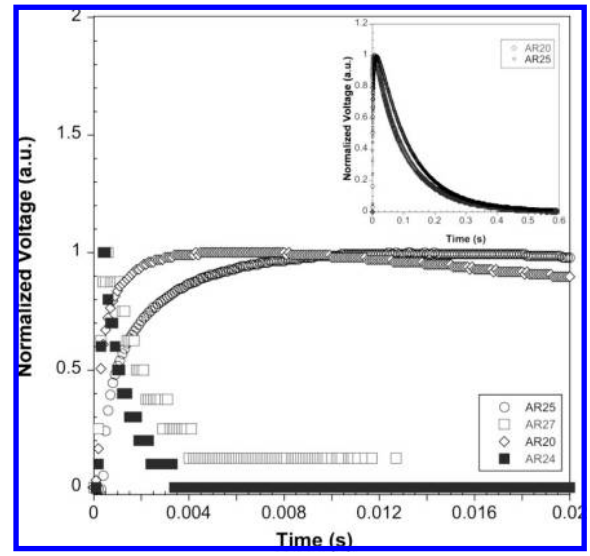


***Figure 11.*** Photovoltage transient decays of the DSSC (Table 4). The inset shows the decay recombination dynamics for AR20/DSSC and AR25/DSSC at longer time scales. The electrolyte was AF19.

$V_{oc}$ values when illuminated at 1 sun. The differences in the voltage can be due to (a) a shift of the $TiO_2$ conduction band with respect to the electrolyte potential or (b) differences in the $e^-$−$TiO_2$/electrolyte$^+$ recombination reaction. The former hypothesis can be discarded due to the fact that a change in the $TiO_2$ conduction band position implies also a shift in the cell charge density as demonstrated previously by other authors.[65−69] As can be seen in Figure 10 for all DSSCs the experimental points emerge along the same curve. Thus, in our case, the differences in voltage must be due to an increase in the $e^-$−$TiO_2$/electrolyte$^+$ recombination reaction in devices made using AR24.

The electron recombination dynamics between the photoinjected electrons at $TiO_2$ and the oxidized electrolyte are illustrated in Figure 11. As can be seen the kinetics are 2 orders of magnitude faster for devices made using either AR24 and AR27.

It is obvious that the presence of the electron donor group at the phenanthroline is responsible for the extraordinarily fast electron recombination kinetics between the electrons injected at the semiconductor upon light excitation of the AR24 molecules and the oxidized electrolyte. The origin of such an effect remains unclear, but interestingly, on this series of Ru(II) complexes the presence of a nitrogen-containing group (either the amino or the nitro) affected not only the photoinduced electron injection from the dye excited state into the $TiO_2$

(63) Forneli, A.; Planells, M.; Sarmentero, M. A.; Martinez-Ferrero, E.; O'Regan, B. C.; Ballester, P.; Palomares, E. *J. Mater. Chem.* **2008**, *18*, 1652.
(64) Planells, M.; Forneli, A.; Martínez-Ferrero, E.; Sánchez-Díaz, A.; Sarmentero, M. A.; Ballester, P.; Palomares, E.; O'Regan, B. C. *Appl. Phys. Lett.* **2008**, *92*, 153506.
(65) Bisquert, J.; Zaban, A.; Greenshtein, M.; Mora-Sero, I. *J. Am. Chem. Soc.* **2004**, *126*, 13550.
(66) O'Regan, B. C.; Durrant, J. R. *J. Phys. Chem. B* **2006**, *110*, 8544.
(67) O'Regan, B. C.; Durrant, J. R.; Sommeling, P. M.; Bakker, N. J. *J. Phys. Chem. C* **2007**, *111*, 14001.
(68) O'Regan, B. C.; Scully, S.; Mayer, A. C.; Palomares, E.; Durrant, J. R. *J. Phys. Chem. B* **2005**, *109*, 4616.
(69) Zaban, A.; Greenshtein, M.; Bisquert, J. *ChemPhysChem* **2003**, *4*, 859.

conduction band, but also the charge transfer reaction between the electrons at the semiconductor film and the iodine/iodide electrolyte.

## Conclusion

We have demonstrated that for the design and synthesis of heteroleptic Ru(II) complexes the presence of substituents on one of the aromatic ligands coordinated to the ruthenium atom has a strong influence not only on the molecule spectroscopic and electrochemical properties but also on the device performance. In fact, we have demonstrated that in the case of the ruthenium complex bearing an amino moiety or a nitro group the molecule affects dramatically the open circuit voltage of the cell. Although a more detailed study is probably needed to find the mechanisms that are deactivating the electron injection on these devices too, we have shown that the low device performance is influenced by the acceleration of the electron transfer dynamics between the photoinjected electrons and the oxidized electrolyte. For devices made using the phenanthroline-substituted heteroleptic Ru(II) complexes the reaction is 2 orders of magnitude faster when compared to that of N719 (data not shown) and AR20 or AR25.

We believe that the results presented in this paper have important implications for the future design of new ruthenium heteroleptic complexes that attempt to achieve higher open circuit voltages in the DSSC without reducing the photocurrent, using electron-donating or -withdrawing groups to control the photophysical properties of the molecules. However, those modifications, as in our case, could lead instead to a poor device performance by the enhancement of undesirable interfacial transfer reactions.

**Acknowledgment.** Financial support from the Spanish MEC is gratefully acknowledged (CONSOLIDER-HOPE 0007-2007 project). E.M.F. thanks the MEC for a Juan de la Cierva fellowship. B.O. and E.P. thank the EU-FP6 OrgaPVNet project for funding. E.P. and A.R. are also grateful to the ICIQ Foundation for financial support.

JA800513M